Preparation and Transport Properties of New Oxide Ion Conductors $KNb_{1-x}Mg_xO_{3-\delta}$ by High Temperature and Pressure

Liping Li,[†,‡] Guangshe Li,*[,§] Jun Xiang,[†] R. L. Smith Jr.,[§] and H. Inomata[§]

Department of Physics, Jilin University, Changchun 130023, P. R. China, Research Center of Supercritical Fluid Technology, Department of Chemical Engineering, Tohoku University, Sendai 980-8579, Japan, and Department of Materials Science, California Institute of Technology, Pasadena, California 91125

Received May 17, 2002. Revised Manuscript Received October 22, 2002

A series of oxide ion conductors $KNb_{1-x}Mg_xO_{3-\delta}$ ($x = 0.05-0.30$) were prepared at a temperature of 870 °C and a pressure of 4.0 GPa. All samples were thermodynamically stable at ambient pressure and crystallized in an orthorhombic perovskite structure. The lattice volume enlarged with increment of dopant level, which was associated with the ionic substitution, variation of the relative content of oxygen vacancy Vö, and defect associations $\{Mg_{Nb}'''Vö\}$, as well as an increase of disorder in Mg^{2+}/Nb^{5+} distribution at B-sites of perovskite lattice. At higher temperatures, $KNb_{1-x}Mg_xO_{3-\delta}$ underwent phase transitions from orthorhombic to tetragonal, pseudocubic, and cubic in sequence, as confirmed by DTA and high-temperature Raman spectra. No thermal effects associated with the decomposition reactions were observed in $KNb_{1-x}Mg_xO_{3-\delta}$ during the successive heating process up to 1000 °C. The high-temperature phase had a relatively high structural stability. Impedance spectra of $KNb_{1-x}Mg_xO_{3-\delta}$ showed bulk and grain boundary conduction. The total conduction was determined to be predominately ionic, while the p-type electronic contribution was extremely small. $KNb_{0.90}Mg_{0.10}O_{2.85}$ was found to provide a highly conductive phase with a conductivity of $\sigma_{700°C} = 1.10 \times 10^{-3}$ S·cm^{-1}. Further, the ionic conductivity data for $KNb_{1-x}Mg_xO_{3-\delta}$ were separated into two linear ranges, corresponding to the pseudocubic and cubic phases, respectively. The variations of conductivity and activation energy for both pseudocubic and cubic phases can be explained in terms of the relative content of the oxygen vacancy and defect associations, delocalization of partial oxygen vacancies, and an order−disorder transition.

Introduction

Perovskite oxides possess a structural unit of ABO_3, in which A represents a larger ion with 12-fold coordination with oxygen ions and B is a smaller ion locating at the octahedral centers.[1] Oxide materials of such structures often show interesting phase transitions and physical properties. $KNbO_3$ is a prototype perovskite ferroelectric material exhibiting phase transitions similar to $BaTiO_3$: from ferroelectric rhombohedral to orthorhombic at −63 °C, to tetragonal at 215 °C, and finally to paraelectric cubic phase at 428 °C.[1] At high pressures, $KNbO_3$ undergoes several irreversible phase transitions,[2] but they are substantially different from those that appeared at higher temperatures. In addition, perovskite structures can be accommodated by doping various kinds of ions at A-sites or B-sites; in this way, structural evolutions and physical properties can be effectively controlled. For example, A-site substitutions in $KNbO_3$ usually lead to a semiconducting behavior,[3] while an oxide ion conduction can be activated when B-site Nb^{5+} is partially replaced by lower valence ions such as Al^{3+}.[4] Similar to other oxide ion conductors, a break is observed in the conductivity data of $KNb_{1-x}Al_xO_3$, which is ascribed to the order−disorder transition of the oxygen vacancies in perovskite lattice.[4]

Dopants in the perovskite oxides alter the microstructures and, furthermore, the physical properties mainly in two ways. The first way is to change the oxygen vacancy concentration in the parent lattice under aliovalent substitution, which forms the possible passages for oxide ion hopping. The second way is to create a large lattice distortion under isovalent substitution with a large difference in ionic size, which produces anti-Frenkel defects and lattice volume variations. In general, a defective perovskite phase with the larger lattice parameters probably shows a higher ionic conductivity.

* Corresponding author. Current address: C302 BNSN, Brigham Young University, Provo UT 84602. E-mail: guangshe@hotmail.com.
† Jilin University.
‡ California Institute of Technology.
§ Tohoku University.

(1) Fontana, M. D.; Metrat, G.; Servoin, J. L.; Gervais, F. *J. Phys.* C **1984**, *16*, 483.
(2) Shen, Z. X.; Hu, Z. P.; Chong, T. C.; Beh, C. Y.; Tang, S. H.; Kuok, M. H. *Phys. Rev.* B **1995**, *52*, 3976.
(3) (a) Hamada, D.; Machida, M.; Sugahara, Y.; Kuroda, K. *J. Mater. Chem.* **1996**, *6*, 69. (b) Kopnin, E. M.; Istomin, S. Y.; Dyachenko, O. G.; Antipov, E. V.; Bordet, P.; Capponi, J. J.; Chaillout, C.; Marezio, M.; Debrion, S.; Souletie, B. *Mater. Res. Bull.* **1995**, *30*, 1379.
(4) Thangadurai, V.; Subbanna, G. N.; Shukla, A. K.; Gopalakrishnan, J. *Chem. Mater.* **1996**, *8*, 1302.

10.1021/cm020582e CCC: $25.00
Published on Web 01/25/2003

As a consequence, strong correlation can be expected between the physical properties and microstructures in perovskite oxides. Busse et al.[5] prepared Mg-doped $KNbO_3$ (0.1 wt % MgO) crystals and found that the absorption loss of the doped sample for the blue light is 40% lower than that of undoped samples, while the infrared absorption is greatly enhanced upon Mg doping. The substitution of Mg^{2+} at B-sites in perovskite lattices can significantly improve the electrical property; e.g., it has been found that enhancement of magnetoresistance occurs in $La_{1-x}Sr_xMn(Mg)O_3$,[6] while for perovskite La(Pr)GaO_3-based electrolytes, addition of Mg^{2+} at B-sites is believed to be one of the most effective methods for increasing the ionic conductivity.[7] Even though $KNbO_3$ has several phase transitions under external fields, however, there are few reports on the phase transitions and transport properties in $KNbO_3$ with B-site Nb^{5+} being partially replaced by Mg^{2+}, which may be due to common problems arising from the phase separation processes during the preparation of Mg niobate-based perovskite oxides.[8]

Mg^{2+} has chemical characteristics that allow it to be easily hydrated and carbonated.[9] Its ionic size (1.34 and 0.72 Å in 12- and 6-fold coordination, respectively) might favor its occupation at A-sites or B-sites in perovskite lattices on the basis of tolerance factor consideration. However, the preparation of such perovskite oxides is rather complex and difficult.[10,11] For example, to obtain the samples containing Nb^{5+} and Mg^{2+} at B-sites in single-phase form, a two-step sintering process with a very long reaction time is necessary.[11] In the synthesis route, the columbite structure compound $MgNb_2O_6$ is a key intermediate phase.[8a] An increase of MgO content in the starting materials usually decreases the relative content of perovskite phase in the final products by forming several separated phases.[11c,d] In addition, Mg^{2+} and Nb^{5+} distribute simultaneously at B-sites in the perovskite lattices (such as $Pb(Nb_{2/3}Mg_{1/3})O_3$ (PMN)),[11g] usually giving excellent ferroelectric properties while the oxide ion conduction in them is considerably poor. Kharton et al.[12] reported on the oxide ion conduction in $LaGa_{0.85-x}Mg_{0.15}(Mg_{0.66}Nb_{0.33})_xO_{3-y}$ ($x = 0.00-0.20$) produced via solid-state reactions at ~1400 °C for 40 h. They found that the ionic conductivity decreases with increasing dopant content, and the samples contain a pronounced amount of impurity phases. Even though such single-phase perovskite oxides could be obtained using a little more complex procedure, X-ray and neutron diffraction methods have not been able to distinguish Nb^{5+} and Mg^{2+} at B-sites (such as in cubic perovskite lattice $Pb(Mg_{1/3}Nb_{2/3})O_3$),[11e,f] and therefore, the local oxygen species or vacancies around Nb^{5+} and Mg^{2+} as well as their effects on the properties remain unclear. With regard to the problems mentioned above, three questions can be raised: (i) Are there any single-step preparation methods for single-phase perovskite oxides with Nb^{5+} and Mg^{2+} at B-sites? (ii) If such methods exist, then what would be the structural stability of the products? (iii) Would the products exhibit any enhancement in ionic conduction having such a lattice? The objective of the present work is to attempt to address these questions.

In this paper, we prepared single-phase $KNb_{1-x}Mg_xO_{3-\delta}$ ($x = 0.05-0.30$) directly by high temperature and pressure and determined the structural stability and oxide ion conduction within this perovskite lattice.

Experimental Section

Analytic reagent grade chemicals $KHCO_3$, MgO, and Nb_2O_5 were used as the starting materials. They were weighed according to the molar ratios of $KNb_{1-x}Mg_xO_{3-\delta}$ ($x = 0.05$, 0.10, 0.15, 0.25, 0.30). After the mixtures were thoroughly ground, each sample was preheated at 700 °C for 5 h at ambient pressure to remove the carbonate species absorbed on the sample surface and to initiate partial reactions. The preheated samples analyzed with a powder X-ray diffraction were mixtures containing component oxides. Each sample was placed into a high-pressure chamber as described in a previous reference.[13] A belt-type apparatus was used for sample preparation. The pressure was set to 4.0 GPa, and then the temperature was increased gradually to 870 °C. After being kept at these conditions for 40 min, the specimens were quenched to room temperature under high pressure. Finally, the pressure was released and the pellet samples were obtained.

Powder X-ray diffraction data for the samples were collected at room temperature on a Rigaku 12kW copper rotating anode X-ray diffractometer. The scan rate was 0.3° 2θ/min. Silica powder (99.99% pure) was used as the internal standard for peak position determination. The lattice parameters for the samples were calculated by least-squares methods. Simultaneous differential thermal analysis (DTA) and thermogravimetric (TG) curves of the samples were recorded on a PE-DTA 1700-TGA7 PC thermoanalyzer at a heating rate of 10 °C/min in air. The compositions for the sample surfaces were measured by X-ray map using scanning electron spectroscopy (JEOL JEM 2000-FX).

Raman spectra of the samples were recorded at a resolution of 2 cm^{-1} on a Dilor Omars 89 spectrometer with an Ar^+ ion laser using an excitation wavelength of 488 nm.

The opposite sides of the pellet samples were coated with silver paste and heated to 550 °C in air for 0.5 h to remove completely the organic components in the paste. The ionic conductivities for the pellet samples were measured using a Solartron 1260 impedance/gain-phase analyzer with the alternating current having a frequency between 10 Hz and 9 MHz at an amplitude of 50 mV in the temperature range of 400−800 °C in air. The impedance spectra were also measured

(5) Busse, L. E.; Goldberg, L.; Surette, M. R.; Mizell, G. *J. Appl. Phys.* **1994**, *75*, 1102.
(6) Anane, A.; Dupas, C.; Le Dang, K.; Renard, J. P.; Veillet, P.; Pinsard, L.; Revcolevschi, A. *Appl. Phys. Lett.* **1996**, *69*, 1160.
(7) (a) Ishihara, T., Matsuda, H., Takita, Y., *J. Am. Chem. Soc.* **1994**, *116*, 3801. (b) Huang, K. Q.; Goodenough, J. B. *J. Alloys Compd.* **2000**, *303*, 454. (c) Goodenough, J. B.; Huang, K. Q. U.S. 6004688 A 21 December, 1999.
(8) (a) Narendar, Y.; Messing, G. L. *J. Mater. Res.* **1999**, *14*, 3921. (b) Swartz, S. L.; Shrout, T. R. *Mater. Res. Bull.* **1982**, *17*, 1245.
(9) Huang, K. Q.; Tichy, R. S.; Goodenough, J. B. *J. Am. Ceram. Soc.* **1998**, *81*, 2565.
(10) (a) Fiquet, G.; Devaele, A.; Andrault, D.; Kunz, M.; Le Bihan, T. *Geophys. Res. Lett.* **2000**, *27*, 21. (b) Yamazaki, D.; Kato, T.; Yurimoto, H.; Ohtani, E.; Toriumi, M. *Phys. Earth Planet. Inter.* **2000**, *119*, 299.
(11) (a) Ananta, S.; Thomas, N. W. *J. Eur. Ceram. Soc.* **1999**, *19*, 2917. (b) Ananta, S.; Thomas, N. W. *J. Eur. Ceram. Soc.* **1999**, *19*, 155. (c) Su, W. F. A. *Mater. Chem. Phys.* **2000**, *62*, 18. (d) Lee, D. Y.; Yoon, S. J.; Yeo, J. H.; Nahm, S.; Paik, J. H.; Whang, K. C.; Ahn, B. G. *J. Mater. Sci. Lett.* **2000**, *19*, 131. (e) Bonneau, P.; Garnier, P.; Husson, E.; Morell, A. *Mater. Res. Bull.* **1989**, *24*, 201. (f) Bonneau, P.; Husson, E.; Morell, A. *Proceedings of the 1st European Ceramic Society Conference*, Maastricht, The Netherlands, 1989. (g) Escribano, P.; Beltran, H.; Cordoncillo, E.; Garcia-Belmonte, G.; Ruiz, L.; Gonzalez-Calbet, J. H.; West, A. R. *Chem. Mater.* **2001**, *13*, 415.
(12) Kharton, V. V.; Yaremchenko, A. A.; Viskup, A. P.; Mather, G. C.; Naumovich, E. N.; Marques, F. M. B. *Solid State Ionics* **2000**, *128*, 79.
(13) Lu, D.; Li, L.; Miao, J.; Liu, H.; Su, W. *Rev. High-Pressure Sci. Technol.* **1998**, *7*, 1031.

at different oxygen partial pressures around that of the oxygen in air. The recorded impedance data were fit to an equivalent circuit model using the least-squares refinement program EQUIVCRT.[14]

Results

Structural Characteristics of $KNb_{1-x}Mg_xO_{3-\delta}$ at Room Temperature. $KNb_{1-x}Mg_xO_{3-\delta}$ ($x = 0.05-0.30$) samples could not be prepared in single phase by solid-state reactions at ambient pressure. XRD data (not shown) analysis indicated that the products obtained by sintering the preheated mixtures at 1000 °C for 32 h and with several intermediate grindings were mixtures containing a main perovskite phase and some unknown impurity phases. Prolonged reaction time had no pronounced influence on the relative content of the mixed phases as estimated from the relative intensity of the most intensive XRD peaks. This is similar to that found for preparation of $K_{1-x}Ba_xNbO_3$ ($0.2 < x < 0.5$).[3b] In this work, we used high temperature and pressure to prepare single-phase $KNb_{1-x}Mg_xO_{3-\delta}$ samples in a single step.

Figure 1 shows XRD patterns of the samples $KNb_{1-x}Mg_xO_{3-\delta}$ ($x = 0.05-0.30$) synthesized at 870 °C and 4.0 GPa. Most of the XRD data for the samples consisted of several split diffraction peaks, which indicated that the present samples had a low symmetric structure. To determine the structure characteristics of these samples, we took undoped $KNbO_3$ as a reference for comparison. At low temperatures, $KNbO_3$ crystallizes in rhombohedral or orthorhombic structures.[2] The rhombohedral phase has the characteristic diffraction lines, such as single lines (012) and (024) at about 23 and 47°, and double lines (110)/(104), (202)/(006), and (122)/(116) at about 33, 41, and 53°, respectively. From Figure 1, it can be seen that the samples exhibited double lines at about 23 and 47°. Therefore, the samples obtained cannot be indexed in rhombohedral. Instead, we found that the XRD data in Figure 1 matched well with the standard data for orthorhombic $KNbO_3$.[15] It is noted that when the dopant content was lower than $x = 0.30$, no diffraction peaks associated with impurity phases such as $MgNb_2O_6$ and $Mg_4Nb_2O_9$ were observed. These impurity phases are, however, key intermediates for the formation of single-phase perovskite oxides (such as $Pb(Nb_{2/3}Mg_{1/3})O_3$) containing Nb^{5+} and Mg^{2+} at B-sites.[8b,16] When the dopant content was larger than $x = 0.30$, some impurity phases were observed (not shown). The indexing of the XRD data in Figure 1 for these single-phase samples indicated that these orthorhombic perovskite structures had a space group of *Cm*2*m* (*38*). No weak and broad superlattice peaks associated with the long-range ordering distribution of oxygen vacancies were observed. The maximum diffraction intensity at ~32° was contributed by three peaks (020), (200), and (111); it was difficult to obtain the exact line width for these peaks due to their much closer

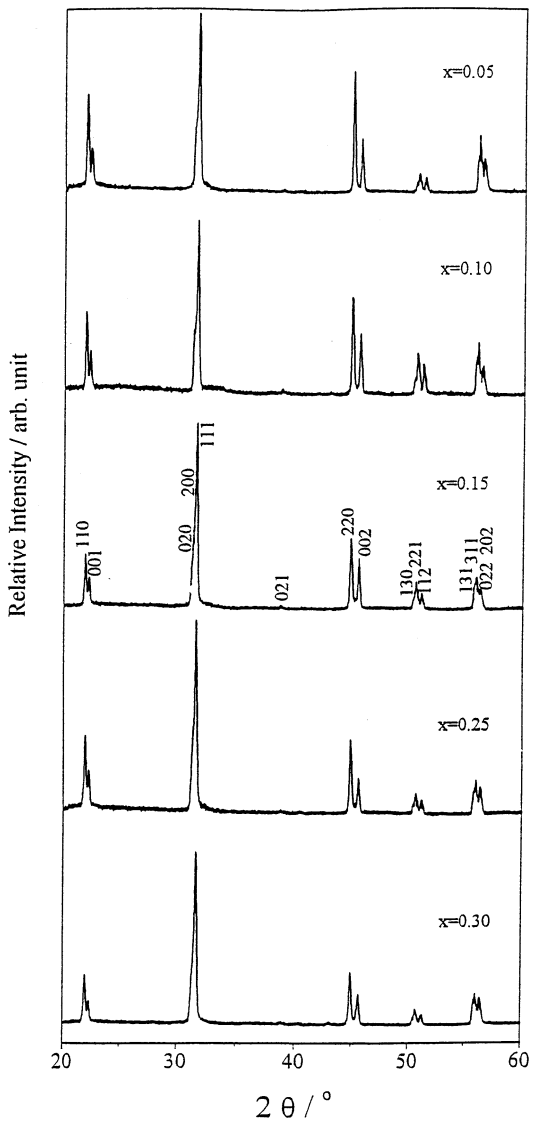

Figure 1. XRD patterns for $KNb_{1-x}Mg_xO_{3-\delta}$ ($x = 0.05-0.30$) prepared directly at 870 °C and 4.0 GPa.

d-spacing values. However, both peaks (220) and (002) centered at ~45° were well separated. Figure 2 shows the relationship between line width of the peak (002) and dopant content. With increasing dopant content, the diffraction peak (002) broadened.

The relationship between lattice volume and dopant content is shown in Figure 3. The lattice volume increased with the dopant content of Mg^{2+}, which seemed to be consistent with the relative ionic size of Mg^{2+} to Nb^{5+} ($r_{Nb(V)} = 0.72$ Å in 6-fold coordination).[17] However, as shown in Figure 3, the relationship between lattice volume and dopant content deviated from the Vegard law. A similar nonlinear relationship has been found in solid solutions $Ce_{1-x}RE_xO_{2-y}$ (RE = Eu, Tb).[18] The reason for this nonlinear relationship will be given in the Discussion section.

Figure 4 shows Raman spectra of the $KNb_{1-x}Mg_xO_{3-\delta}$ samples recorded at room temperature. All samples had Raman bands similar to those of undoped $KNbO_3$,[2,19] namely, a weak sharp band at ~190 cm^{-1}, broad bands

(14) Boukamp, B. B. *Equivalent Circuit*; University of Twente: Twente, The Netherlands, 1988.
(15) McLune, W. F., Ed. *Powder Diffraction File; Inorganic Phases*; JCPDS International Centre for Powder Diffraction Data: Swarthmore, PA, 1989; Card No. 32-822.
(16) (a) Hong, Y. S.; Park, H. B.; Kim, S. J. *J. Eur. Ceram. Soc.* **1998**, *18*, 613. (b) Joy, P. A.; Sreedhar, K. *J. Am. Ceram. Soc.* **1997**, *80*, 770.
(17) Shannon, R. D. *Acta Crystallogr., Sect. A* **1976**, *32*, 751.
(18) Li, L.; Li, G.; Che, Y.; Su, W. *Chem. Mater.* **2000**, *12*, 2567.

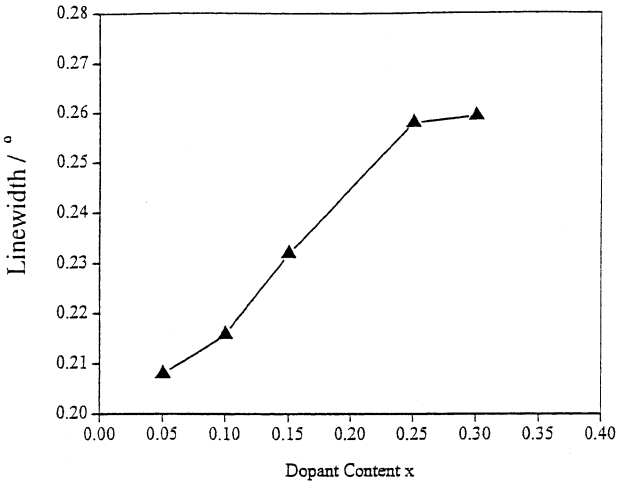

Figure 2. Relationship of line width for diffraction (002) and dopant content x in $KNb_{1-x}Mg_xO_{3-\delta}$ ($x = 0.05-0.30$).

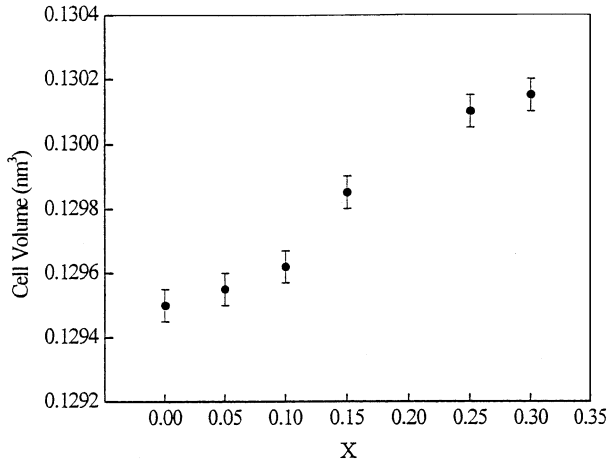

Figure 3. Relationship between lattice volume and dopant content x for $KNb_{1-x}Mg_xO_{3-\delta}$ ($x = 0.05-0.30$).

at 280, 530, and 580 cm^{-1}, and a weak peak at ~830 cm^{-1}. According to the literature,[2] the Raman bands in Figure 4 can be assigned. The weak band at ~190 cm^{-1} is ascribed to the mixed modes of A_1(TO), A_l(LO), and B_2(TO). The broad bands at about 280 and 530 cm^{-1} are associated with the B_1(TO) mode, while the band at ~580 cm^{-1} is due to the A_1(TO) mode and that at ~830 cm^{-1} is due to the A_1(LO) mode. It should be mentioned that $MgCO_3$, Nb_2O_5, and most of the intermediates in the $MgO-Nb_2O_5$ system are Raman active.[20] However, no Raman bands from these impurity phases were observed. These results clearly indicated that the present samples $KNb_{1-x}Mg_xO_{3-\delta}$ ($x = 0.05-0.30$) crystallized in the same orthorhombic structure as that for undoped $KNbO_3$. The samples did not show the presence of impurity phases such as pyrochlore in the preparation of PMN,[8b] which is probably related to the improved reactivity and the great enhancement of the phase transformation rate of pyrochlore to perovskite by an additional driving force provided by high

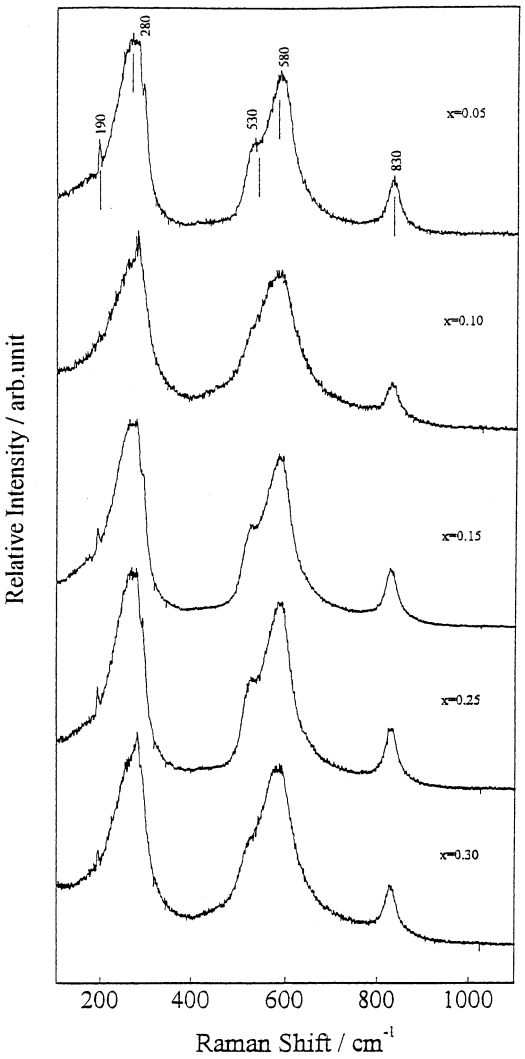

Figure 4. Room-temperature Raman spectra for $KNb_{1-x}Mg_xO_{3-\delta}$ ($x = 0.05-0.30$).

pressures.[21] Many high-pressure phase transitions are reversible when pressure is lowered; however, once the formation reactions are completed at high pressures, especially at high temperatures, the atom arrangements, even in a metastable form, can be stabilized at ambient conditions because the thermodynamically spontaneous reverse reaction is kinetically sluggish or unfavored at lower temperatures.[21d] The preparation of perovskite lattice $KNb_{1-x}Mg_xO_{3-\delta}$ is also associated with its tolerance factor at ~1.01, nearly the same as that of the undoped $KNbO_3$.

Structural Stability of $KNb_{1-x}Mg_xO_{3-\delta}$ at Ambient Pressure and Elevated Temperatures. Single phases of $KNb_{1-x}Mg_xO_{3-\delta}$ were prepared by high temperature and pressure. It is necessary to identify their structural stability at ambient pressure and elevated temperatures. We annealed the samples in air at 900 °C for 5 h and did not observe any change in the XRD patterns (not shown). This fact indicated that the present orthorhombic perovskite structures were kinetically stable at ambient pressure. In general, at elevated

(19) (a) Quittet, A. M.; Bell, M. I.; Krauzman, M.; Raccah, P. M. *Phys. Rev.* B **1976**, *14*, 5068. (b) Bozinis, D. G.; Hurrell, J. P. *Phys. Rev.* B **1976**, *13*, 3109.

(20) (a) Gillet, P. *Am. Mineral.* **1993**, *78*, 1328. (b) Dobal, P. S.; Dixit, A., Katiyar, R. S.; Choosuwan, H.; Gao, R.; Bhalla, A. S. *J. Raman Spectrosc.* **2002**, *33*, 121. (c) Camargo, E. R.; Longo, E.; Leite, E. R. *J. Sol−Gel Sci. Technol.* **2000**, *17*, 111. (d) Bruck, E.; Route, E. K.; Raytmakers, R. J.; Feigelson, R. S. *J. Cryst. Growth* **1993**, *128*, 842.

(21) (a) McMillan, P. F. *Nat. Mater.* **2002**, *1*, 19, (b) Lee, J. H.; Chiang, Y. M. *J. Electroceram.* **2001**, *6*, 7. (c) Demazeau, G. *Chem. Scr.* **1988**, *28*, 21. (d) Yamauchi, H.; Karppinen, M. *Supercond. Sci. Technol.* **2000**, *13*, R33.

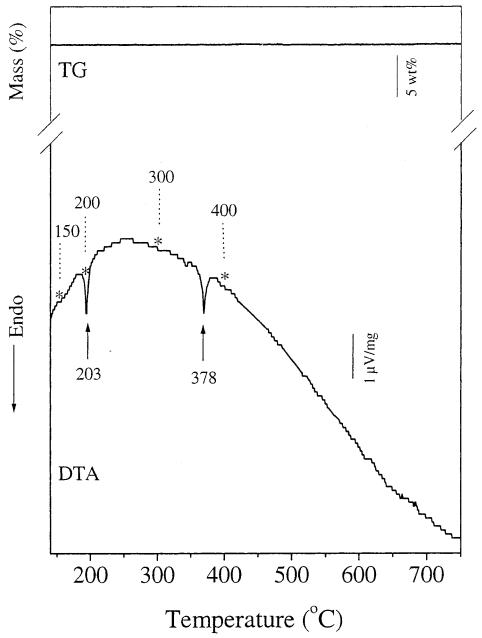

Figure 5. DTA-TG curves for a typical sample $KNb_{0.85}Mg_{0.15}O_{2.78}$. Two endothermic peaks at 203 and 378 °C with no mass variations were ascribed to the phase transitions from orthorhombic to tetragonal and to pseudocubic, respectively. * denotes several points of Raman measurement for identifying both transitions.

temperatures, perovskite oxides or the related lattices of lower symmetry would show several first-order transitions to higher symmetric phases, which are characterized by the transition entropy. An endothermic peak has been observed for a phase transition from tetragonal to cubic in $BaTiO_3$[22] and from monoclinic to cubic in $La_2Mo_2O_9$.[23] The phase stability of $KNb_{1-x}Mg_xO_{3-\delta}$ at elevated temperatures was determined by DTA-TG. Figure 5 shows the DTA-TG curves for a typical sample of $KNb_{0.85}Mg_{0.15}O_{2.78}$ measured in air. Two endothermic peaks centered at about 203 and 378 °C were observed. In the corresponding TG curve, no mass changes were observed. Here, it is hard to distinguish any possible second-order transitions due to the lack of thermal effects; however, these results clearly demonstrated that there were at least two possible high-temperature first-order transitions in $KNb_{0.85}Mg_{0.15}O_{2.78}$, corresponding to the transitions from orthorhom-
bic to tetragonal and from tetragonal to pseudocubic, respectively, which were identified by high-temperature Raman spectra and will be described later. Similar transitions have been found at other compositions of $KNb_{1-x}Mg_xO_{3-\delta}$. During the successive heating process up to 1000 °C, no thermal effects associated with the decomposition reactions were observed in $KNb_{0.85}Mg_{0.15}O_{2.78}$, indicating that the high-temperature phase had a relatively high structural stability. When the temperature was higher than 1077 °C, the $KNb_{0.85}Mg_{0.15}O_{2.78}$ sample melted, accompanied by a large endothermic peak. To identify the high-temperature phases in $KNb_{1-x}Mg_xO_{3-\delta}$, we measured the high-temperature Raman spectra of two typical samples, $KNb_{0.85}Mg_{0.15}O_{2.78}$ and $KNb_{0.70}Mg_{0.30}O_{2.55}$. It should be mentioned that the direct method often used in observing the phase transitions is XRD. However, the broadening effects in the XRD patterns arising from the disordered distribution make it invalid to distinguish the high-temperature phases, especially when those high-temperature phases have a relatively high symmetry. Raman spectroscopy has been demonstrated to be a highly sensitive spectroscopic technique to probe the local structures in perovskite lattices such as $KNbO_3$.[2,24]

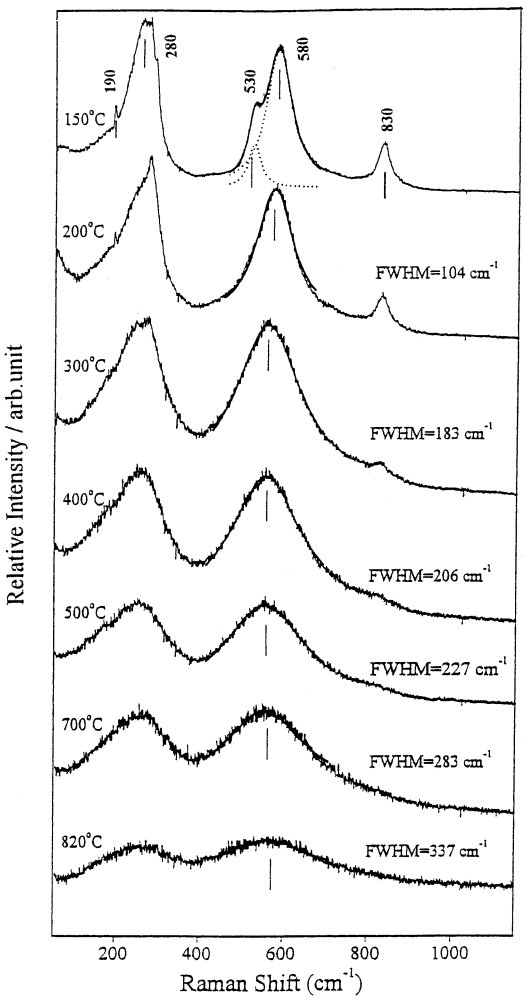

Figure 6. High-temperature Raman spectra for a typical sample $KNb_{0.85}Mg_{0.15}O_{2.78}$. The fwhm for the phonon mode at ~580 cm^{-1} is shown on the corresponding spectrum.

Figure 6 shows the high-temperature Raman spectra for $KNb_{0.85}Mg_{0.15}O_{2.78}$. The Raman spectra recorded at temperatures below 150 °C were nearly the same as the room-temperature spectrum. The phonon modes at about 530 and 580 cm^{-1} could be deconvoluted using Lorentzian shape functions. These results were consistent with the orthorhombic phase. At 200 °C, a point that just falls in the regime for the first endothermic peak in Figure 5, the intensity for the weak sharp phonon mode at 190 cm^{-1} decreased, and the mode at

(22) (a) Asiaie, R.; Zhu, W. D.; Akbar, S. A.; Dutta, P. K. *Chem. Mater.* **1996**, *8*, 226. (b) Didomenico, M., Jr.; Wemple, S. H.; Porto, S. P. S.; Bauman, R. P. *Phys. Rev.* **1968**, *174*, 522. (c) Shimooka, H.; Kuwabara, M. *J. Am. Ceram. Soc.* **1996**, *79*, 2983.

(23) Lacorre, P.; Goutenoire, F.; Bohnke, O.; Retoux, R.; Laligant, Y. *Nature* **2000**, *404*, 856.

(24) Naik, R.; Nazarko, J. J.; Flattery, C. S.; Venkateswaran, U. D.; Naik, V. M.; Mohammed, M. S.; Auner, G. W.; Mantese, J. V.; Schubring, N. W.; Micheli, A. L.; Catalan, A. B. *Phys. Rev. B* **2000**, *61*, 11367.

$\sim$280 cm^{-1} became asymmetric, indicating that the orthorhombic phase was not predominant. The phonon mode at 530 cm^{-1} vanished, while the mode at $\sim$580 cm^{-1} became a single mode of high symmetry. We used Lorentzian shape functions to derive the full width at half-maximum (fwhm) of the phonon mode at $\sim$580 cm^{-1}. The fwhm for this mode is shown on the right of Figure 6. It can be seen that the phonon mode at 580 cm^{-1} for $KNb_{0.85}Mg_{0.15}O_{2.78}$ had an fwhm of 104 cm^{-1} at 200 °C. The asymmetric band at $\sim$280 cm^{-1} reflects the presence of asymmetric $Nb(Mg)O_6$ octahedra at B-sites.[25,26] Therefore, the phase transition from orthorhombic to tetragonal in $KNb_{0.85}Mg_{0.15}O_{2.78}$ probably proceeded via the production of asymmetric octahedra for B-site ions.

At 300 °C, a point that is well above the regime for the first endothermic peak in Figure 5, the weak sharp phonon mode associated with the orthorhombic structure disappeared at $\sim$190 cm^{-1} and the phonon modes centered at about 280 and 580 cm^{-1} became two symmetric modes, while the mode at $\sim$830 cm^{-1} was further weakened. Especially, the fwhm for the phonon mode at $\sim$580 cm^{-1} was much broader at 183 cm^{-1} (300 °C) than that at 104 cm^{-1} (200 °C). Therefore, a tetragonal phase was probably formed. At 400 °C, a point that is well above the regime for the second endothermic peak in Figure 5, two highly symmetric phonon modes at about 280 and 580 cm^{-1} were slightly weakened, while the fwhm for the mode at $\sim$580 cm^{-1} increased to 206 cm^{-1}. The mode at $\sim$830 cm^{-1} lost most of its intensity and was too faint to be observed. These results could be associated with a pseudocubic phase.[25] With increasing temperatures above 500 °C, as shown in Figure 6, both phonon modes centered at about 280 and 580 cm^{-1} further broadened and lost intensity, which could be associated with the transition of pseudocubic to cubic. Above 600 °C, both phonon modes further weakened at about 280 and 580 cm^{-1}. The mode at $\sim$830 cm^{-1} disappeared completely. These results were evidence of the formation of a cubic phase. Two similar weak phonon modes are also found for cubic $BaTiO_3$.[27]

High-temperature Raman spectra for $KNb_{0.70}Mg_{0.30}O_{2.55}$ are shown in Figure 7. At temperatures below 150 °C, $KNb_{0.70}Mg_{0.30}O_{2.55}$ gave a very weak phonon mode at $\sim$190 cm^{-1}, which was probably associated with overlapping of some phonon modes and the background under the broadening effect due to an increase of disorder at heavy doping. The phonon mode centered at $\sim$280 cm^{-1} became asymmetric. Both modes at about 530 and 580 cm^{-1} were still observable as deconvoluted by using Lorentzian shape functions shown in Figure 7. These results were associated with an orthorhombic phase below 150 °C. At 300 °C, the weak phonon mode at $\sim$190 cm^{-1} and the stronger one at $\sim$530 cm^{-1} disappeared, while the broad phonon mode at $\sim$580 cm^{-1} became a single mode as fitted by Lorentzian shape functions. Similar to that for $KNb_{0.85}Mg_{0.15}O_{2.78}$, the highly symmetric phonon mode at $\sim$580 cm^{-1} was ascribed to the presence of a tetragonal phase. The fwhm for the phonon mode at $\sim$580 cm^{-1} is shown on the right of Figure 7. At 300 °C, the fwhm of this mode was as wide as 112 cm^{-1}, which showed a jump to 187 cm^{-1} at 400 °C. At 400 °C, the phonon mode at $\sim$830 cm^{-1} became considerably weaker compared with that at 300 °C. These results were probably associated with a pseudocubic phase at 400 °C. Above 600 °C, the broad mode at $\sim$830 cm^{-1} disappeared completely. Both broad phonon modes centered at about 280 and 580 cm^{-1} were shown to have a low S/N ratio and lost intensity gradually with increasing temperature, which was associated with a transition of pseudocubic to cubic phase. It is clear that these transitions were quite similar to those observed for $KNb_{0.85}Mg_{0.15}O_{2.78}$ in Figure 6.

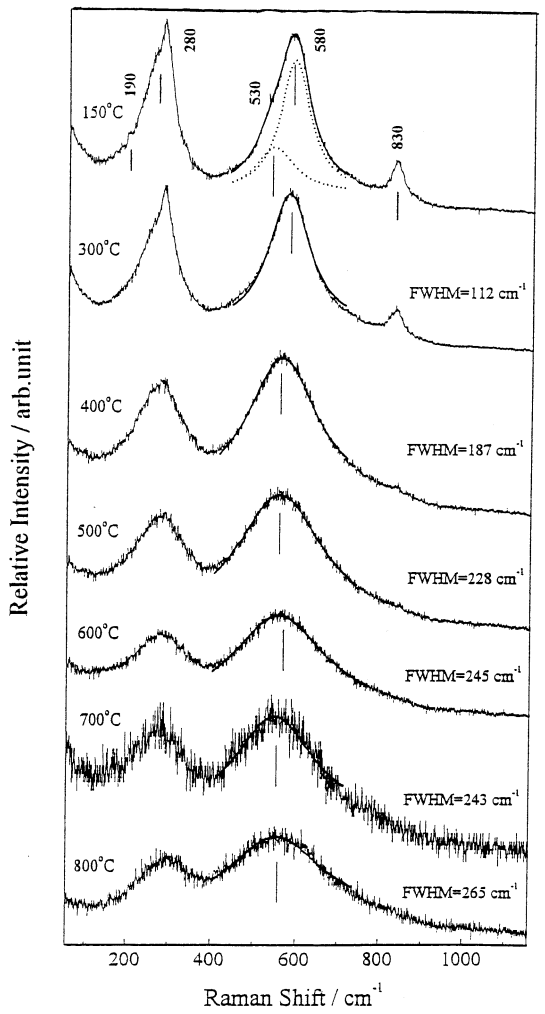

Figure 7. High-temperature Raman spectra for a typical sample $KNb_{0.70}Mg_{0.30}O_{2.55}$. FWHMs are given for the phonon mode at $\sim$580 cm^{-1}. Dashed lines show Lorentzian fits.

Oxide Ion Conduction in $KNb_{1-x}Mg_xO_{3-\delta}$ at Elevated Temperatures. Oxide ion conduction in $KNb_{1-x}Mg_xO_{3-\delta}$ was determined by ac impedance spectroscopy. At temperatures lower than 350 °C, the samples showed extremely large resistance and did not give full arcs. Figure 8 illustrates the impedance spectrum for a typical composition of $KNb_{0.90}Mg_{0.10}O_{2.85}$ that was recorded at 398 °C in air. The impedance data were fit to an equivalent circuit model,[28] in which one Q element and two subcircuits (R and Q in parallel) are

(25) Fontana, M. D.; Kugel, G. E.; Vamvakas, J.; Carabatos, C. *Solid State Commun.* **1983**, *45*, 873.
(26) Clark, I. J.; Takeuchi, T.; Ohtori, N.; Sinclair, D. C. *J. Mater. Chem.* **1999**, *9*, 83.
(27) Fontana, M. P.; Lambert, M. *Solid State Commun.* **1972**, *10*, 1.

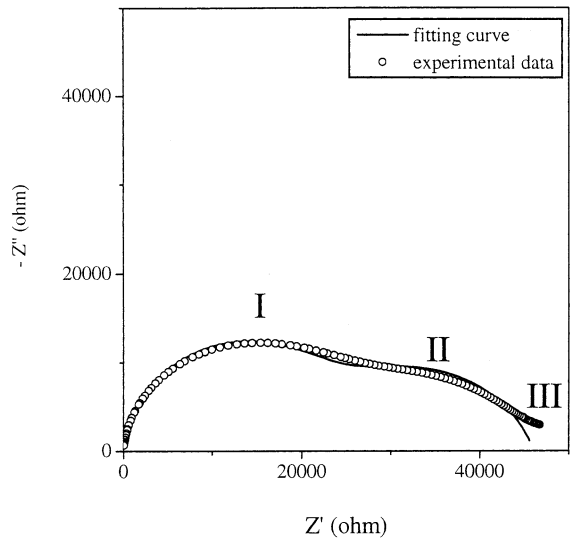

Figure 8. Impedance spectrum for a typical composition of $KNb_{0.90}Mg_{0.10}O_{2.85}$, recorded at 398 °C in air. Solid line shows fit by an equivalent circuit model.

in series with one another, where R represents a resistor and Q is the constant-phase element. The fitting results by this model are also shown in Figure 8. It is seen that the impedance spectrum was mainly composed of two depressed semicircles. The semicircle (I) at higher frequencies can be attributed to the bulk effect, while the intermediate frequency semicircle (II) can be ascribed to the grain boundary conduction. It should be mentioned that, at higher dopant levels, a spike (III) appeared at lower frequencies, which is due to the overall electrode processes. The impedance spectra in Figure 8 can be deconvoluted as overlapped or nonoverlapped semicircles. Mukundan et al.[29] tried fitting the conductivity data of orthorhombic perovskite $SrCe_{0.95}Yb_{0.05}O_{2.975}$ using overlapped semicircles, but the values of their activation energies exhibited large scatter.

In this work, we emphasized the relationship between total conductivity and dopant content by estimating the resistance with nonoverlapped semicircles. The conductivity for $KNb_{1-x}Mg_xO_{3-\delta}$ was determined by the intersection of the semicircles on the real part of the impedance axis. Figure 9 gives ln σT and $1/T$ plots of $KNb_{1-x}Mg_xO_{3-\delta}$. It can be seen that the total conductivity data for all samples were separated into two linear regions. That is, the conduction at lower temperatures had a lower activation energy, while above the transition temperatures, there was a break in the conductivity data, which gave an increase in the conductivity and activation energy. To further confirm the dominant ionic conduction in $KNb_{1-x}Mg_xO_{3-\delta}$ under the present experimental conditions, we measured the impedance spectra of a typical sample $KNb_{0.90}Mg_{0.10}O_{2.85}$ at 500 °C under several oxygen partial pressures around that of air. The dependence of the conductivity on the oxygen partial pressure is shown in Figure 10. No pronounced variation was observed in the conductivity data under the selected oxygen partial pressures. Even though there was a

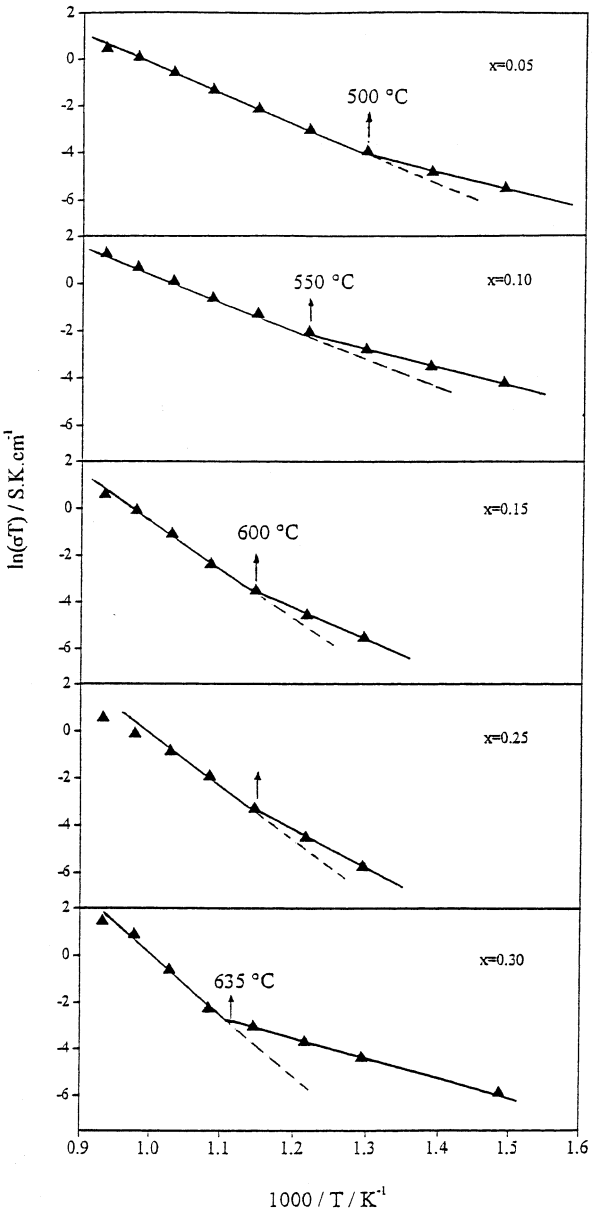

Figure 9. Temperature dependence of total conductivity for $KNb_{1-x}Mg_xO_{3-\delta}$ ($x = 0.05-0.30$).

slight increase in the conductivity at higher oxygen partial pressures, as shown in Figure 10, the slope $\partial \log \sigma / \partial \log PO_2$ in this oxygen partial pressure region was much less than $^1/_4$ or $^1/_6$, the characteristic regime for p-type electronic conduction.[30] The weak PO_2 dependence of the conductivity data was thus probably due to the transition regime between the ionic conductivity with no PO_2 dependence and p-type electronic conductivity with slope $\partial \log \sigma / \partial \log PO_2$ a $^1/_4$ or $^1/_6$. Theoretical modeling has been reported on the oxide ion or cation conduction in perovskite lattices.[31] However, it is highly unlikely that cation conduction for the present $KNb_{1-x}Mg_xO_{3-\delta}$, cation conduction associated with K^+, Mg^{2+}, and Nb^{5+}, occurs via cation vacancies. This can be reasoned from the comparison of the measured activation energies and the theoretical values for cation conduction. The activation energies of $KNb_{1-x}Mg_xO_{3-\delta}$

(28) (a) Haile, S. M.; West, D. L.; Campbell, J. *J. Mater. Res.* **1998**, *13*, 1576. (b) Gerhardt, R.; Nowick, A. S. *J. Am. Ceram. Soc.* **1986**, *69*, 641. (c) Macdonald, J. R. *Impedance Spectroscopy*; Wiley: New York, 1987.

(29) Mukundan, R.; Brosha, E. L.; Birdsell, S. A.; Costello, A. L.; Garzon, F. H.; Willms, R. S. *J. Electrochem. Soc.* **1999**, *146*, 2184.

(30) Shimura, T.; Fujimoto, S.; Iwahara, H. *Solid State Ionics* **2001**, *143*, 117.

(31) Islam, M. S. *J. Mater. Chem.* **2000**, *10*, 1027.

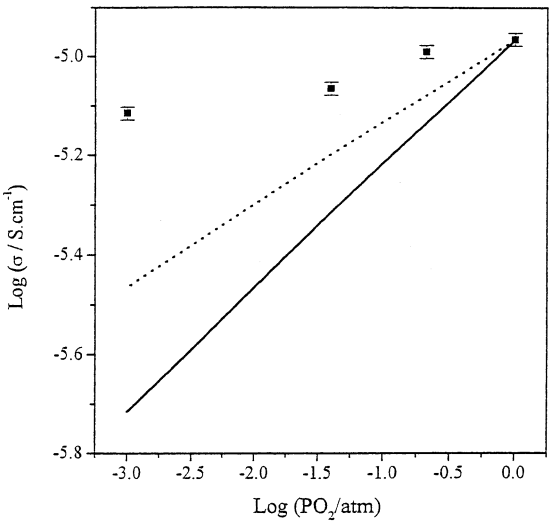

Figure 10. Conductivity dependence on oxygen partial pressure for a typical sample $KNb_{0.90}Mg_{0.10}O_{2.85}$ at 500 °C. Two lines showing $\partial \log \sigma / \partial \log PO_2$ at $^1/_6$ (dotted) and $^1/_4$ (solid) are given to demonstrate the primary ionic nature and extremely small p-type electronic contribution to total conduction in the sample.

Table 1. Conductivities (σ) and Activation Energies (E_a) of $KNb_{1-x}Mg_xO_{3-\delta}$ ($x = 0.00-0.30$) Measured at 500 and 700 °C. [a]Denotes the Data from Ref 4

x	$\sigma_{500°C}$ ($S \cdot cm^{-1}$)	$E_{a500°C}$ (eV)	$\sigma_{700°C}$ ($S \cdot cm^{-1}$)	$E_{a700°C}$ (eV)
0.00[a]	1.80×10^{-6}	0.89	3.20×10^{-5}	0.89
0.05	2.54×10^{-5}	0.55	5.50×10^{-4}	0.85
0.10	7.90×10^{-5}	0.58	1.10×10^{-3}	0.83
0.15	5.14×10^{-6}	0.93	3.50×10^{-4}	1.35
0.25	4.15×10^{-6}	1.13	4.30×10^{-4}	1.40
0.30	1.65×10^{-5}	0.57	5.50×10^{-4}	1.73

were relatively lower having values of around 1.0 eV, which is characteristic of oxygen migration. Assuming that cation conduction was present in $KNb_{1-x}Mg_xO_{3-\delta}$, the extremely large ionic size of 1.64 Å for K^+ at the A-site of the perovskite lattice would probably yield an activation energy larger than 4.0 eV.[31] For the B-site ions such as Mg^{2+} and Nb^{5+}, the migration energy along the diagonal direction ⟨110⟩ would be even higher and would have a value, most likely, around 14 eV. Therefore, cation vacancy formation and furthermore cation conduction by vacancy migration between the neighboring sites should be highly unfavorable as expected for the close-packed perovskite lattice of $KNb_{1-x}Mg_xO_{3-\delta}$. In consideration of the weak oxygen partial pressure relationship of the conductivity data, it is reasonable that the present samples were a mixed-type conductor of primary oxide ion and traces of electron holes. Similarly, primary oxide ion conduction as well as p-type electronic conduction have been found in several perovskite oxides, such as in Mg-doped $LaGaO_3$.[7b,32]

The conductivities and activation energies for $KNb_{1-x}Mg_xO_{3-\delta}$ at 500 and 700 °C are listed in Table 1. The literature data[4] for $KNbO_3$ at both temperatures are also shown for comparison. At 500 °C, the conductivity increased with the dopant content from 1.80×10^{-6} $S \cdot cm^{-1}$ at $x = 0.00$ to 7.90×10^{-5} $S \cdot cm^{-1}$ at $x = 0.10$. When the dopant content was above $x = 0.10$, the conductivity for $KNb_{1-x}Mg_xO_{3-\delta}$ decreased to 4.15×10^{-6} $S \cdot cm^{-1}$ at $x = 0.25$. Then, the conductivity increased to 1.65×10^{-5} $S \cdot cm^{-1}$ at $x = 0.30$. Correspondingly, the activation energy decreased with dopant content from $E_a = 0.89$ eV at $x = 0.00$ to 0.55 eV at $x = 0.05$. Further increasing dopant content led to an increase of the activation energy to $E_a = 1.13$ eV at $x = 0.25$. Then the activation energy decreased to $E_a = 0.57$ eV at $x = 0.30$.

The conductivity data at 700 °C for $KNb_{1-x}Mg_xO_{3-\delta}$ were much enhanced in comparison with those at 500 °C. With increasing dopant content, the conductivity increased from 3.20×10^{-5} $S \cdot cm^{-1}$ at $x = 0.00$ to 1.10×10^{-3} $S \cdot cm^{-1}$ at $x = 0.10$. When the dopant content was higher than $x = 0.10$, the conductivity decreased to 3.50×10^{-4} $S \cdot cm^{-1}$ at $x = 0.15$ and then increased to 5.50×10^{-4} $S \cdot cm^{-1}$ at $x = 0.30$. Correspondingly, the activation energy decreased slightly from $E_a = 0.89$ eV at $x = 0.00$ to 0.83 eV at $x = 0.10$. There was a sharp increase of activation energy to $E_a = 1.35$ eV at $x = 0.15$, and then the activation energy increased continuously to $E_a = 1.73$ eV at $x = 0.30$. From Table 1, $KNb_{0.90}Mg_{0.10}O_{2.85}$ was found to exhibit most favorable conduction characteristics such as a relatively high conductivity and low activation energy.

Discussion

Correlation of Lattice Volume Variation with Defect Characteristics of $KNb_{1-x}Mg_xO_{3-\delta}$. The lattice volume variation with dopant content for $KNb_{1-x}Mg_xO_{3-\delta}$ could be explained by taking into account the relative ionic size of Mg^{2+} to Nb^{5+} and the charge difference. Doping of larger Mg^{2+} at Nb^{5+} sites in $KNbO_3$ produced a larger lattice distortion, which was the main reason for the lattice expansion. On the other hand, owing to a large charge difference between Nb^{5+} and Mg^{2+}, when a fracture of Nb^{5+} was replaced by Mg^{2+}, there should be some negative charge centers formed in a local scale near Mg^{2+}, which could be balanced by oxygen vacancies produced in the perovskite lattice of $KNb_{1-x}Mg_xO_{3-\delta}$. In this case, every two Mg^{2+} ions in lattice would yield three oxygen vacancies Vö. Mg^{2+} probably attracted the oxygen vacancies to the nearest neighboring positions due to the Coulombic forces. Therefore, an inhomogeneous distribution of oxygen vacancies are expected. With an increase in dopant content of Mg^{2+}, the average concentration of oxygen vacancy Vö would increase. As indicated by the relative variations of the conductivity data (Table 1), it is probable that when the dopant content was further increased beyond $x = 0.10$, localized defect associations $\{Mg_{Nb}'''Vö\}$ or oxygen vacancy clusters appeared and their content increased at the expense of mobile oxygen vacancies Vö, as has been found in other solid solutions at higher dopant contents.[33] In contrast to cationic substitution, both oxygen vacancies Vö and defect associations $\{Mg_{Nb}'''Vö\}$ or oxygen vacancy clusters were considered to contribute lattice constraints. It should be mentioned that oxygen vacancies Vö and defect associations $\{Mg_{Nb}'''Vö\}$ have different interactions with the framework ions, and the effect from the

(32) Kharton, V. V.; Yaremchenko, A. A.; Viskup, A. P.; Mather, G. C.; Naumovich, E. N.; Marques F. M. B. *J. Electroceram.* **2001**, *7*, 57.

(33) Lidiard, A. B. In *Handbuch der Physik*; Flugge, S., Ed.; Springer-Verlag: Berlin, 1956; Vol. XX.

oxygen vacancies may be slightly larger than the defect associations in reducing the lattice volume.[17] The cationic substitutions and variations for the relative content of oxygen vacancy Vö and defect associations $\{Mg_{Nb}'''Vö\}$ were therefore assumed to be the main reasons for the nonlinearity in Figure 3. Similar reasons have been proposed to explain the nonlinearity for solid solutions $Ce_{1-x}RE_xO_{2-x}$ (RE = Eu, Tb).[17] However, a linear relationship can be expected when the dopants have a much larger ionic size compared with host ions even in the presence of large amounts of defect associations or oxygen vacancy clusters.[34]

Disordered distribution of Nb^{5+}/Mg^{2+} at B-sites also showed some contribution to the nonlinearity in Figure 3. This is because a large amount of oxygen vacancies Vö or defect associations $\{Mg_{Nb}'''Vö\}$ in $KNb_{1-x}Mg_xO_{3-\delta}$ produced lattice distortion on a small scale, which probably yielded some displacements for Mg^{2+} or Nb^{5+} at B-sites. Taking into account the slightly larger ionic radii of Mg^{2+} than Nb^{5+}, the Nb−O bonds were expected to be shorter than the Mg−O bonds, which should generate a distorted BO_6 octahedra network by a slight lattice expansion. Moreover, the Nb−O bonds are more covalent and are more inflexible in comparison with the Mg−O bonds. Therefore, a partial disorder of Mg^{2+}/Nb^{5+} at B-sites can be expected, as is observed in orthorhombic $BaTiO_3$ and $KNbO_3$.[35] As a result, the oxygen vacancies were probably long-range disordered in $KNb_{1-x}Mg_xO_{3-y}$, in good agreement with the absence of superlattice peaks in Figure 2. Such a disordered distribution was also confirmed by the broadening effect in XRD patterns in Figure 2, even though the broadening effect in XRD could be due to a decrease in particle size or an increase in lattice disorder. In this work, all samples were prepared by high temperature and pressure using commercial oxides of several micrometers in dimension as the starting materials; a decrease in particle size is not a likely explanation. Similar results have been found in $(1 - x)Pb(Mg_{1/3}Nb_{2/3})O_3 - xPbTiO_3$ containing disordered B-site ions due to Ti^{4+} substitution.[36]

Correlation of Phase Transitions with Lattice Disorder in $KNb_{1-x}Mg_xO_{3-\delta}$. $KNb_{1-x}Mg_xO_{3-\delta}$ underwent phase transitions from orthorhombic, to tetragonal, to pseudocubic, and to cubic. The transition from tetragonal to pseudocubic accompanied by the broadened phonon mode at ~580 cm^{-1} (Figures 6 and 7) could be understood in terms of the change from tetragonal mode to the triply degenerated cubic F_{1u} mode.[37] As described above, substitution of Nb^{5+} by the larger Mg^{2+} could give a larger displacement for Nb^{5+}, and the oxygen vacancies adjacent to Mg^{2+} could produce much distorted polyhedra around Nb^{5+}. As a result, $KNb_{1-x}Mg_xO_{3-\delta}$ exhibited phase transitions different from those in undoped $KNbO_3$ at high temperatures.[1] In the latter case, no pseudocubic was obtained. Pseudocubic $KNb_{1-x}Mg_xO_{3-\delta}$ contained a partial lattice order, whereas B-site ions in the cubic phase can be assumed to be distributed disorderly at eight off-center sites along the ⟨111⟩ axes due to the potential energy minimums at these sites.[38] According to group theory analysis, the irreducible representation of 12 optical phonons for the cubic phase (space group $Pm3m$) is $3F_{1\mu} + F_{2\mu}$. All phonon modes for this highly symmetric structure are Raman inactive. Therefore, the phonon modes such as that at 580 cm^{-1} should be forbidden. The presence of these weak modes can be well explained in terms of the disordered arrangements existing in the lattice of $KNb_{1-x}Mg_xO_{3-\delta}$ for such disordered arrangements could result in removal of the inversion symmetry for the O_h point group and thus activate some Raman modes that are originally inactive.[39]

Similar distributions of Mg^{2+} and Nb^{5+} in $KNb_{1-x}Mg_xO_{3-\delta}$ can be expected at one to eight off-center sites along the ⟨111⟩ axes in the presence of some lattice distortions due to the size mismatch of Mg^{2+}/Nb^{5+} at B-sites. In fact, oxygen vacancies or oxygen vacancy clusters adjacent to Mg^{2+} probably give rise to an inhomogeneous distribution of electrical field at B-sites. The different static displacements of Mg^{2+} and Nb^{5+} decreased the local symmetry for B-site ions.[40] Therefore, with increasing temperature, a rapid increase in the disorder of Nb^{5+}/Mg^{2+} at B-sites was favored to preserve a highly symmetric average cubic structure at high temperatures, which was confirmed by the weakened intensity of both phonon modes for the cubic.[41] At higher dopant contents, large amounts of oxygen vacancies Vö and defect associations $\{Mg_{Nb}'''Vö\}$ showed strong interactions with the framework ions and mobile oxygen ions. The transition of order−disorder of oxygen vacancies was thus suppressed. This is probably the main reason for an increase in transition temperature of pseudocubic to cubic with increasing dopant content shown in Figure 9.

Correlation of Oxide Ion Conduction with Defect Characteristics and Lattice Disorder in $KNb_{1-x}Mg_xO_{3-\delta}$. We addressed first the increased activation energy and conductivity data shown in Figure 9 for the cubic phase in comparison with the pseudocubic phase. Oxide ion conduction in perovskite lattice was achieved by oxide ions passing through a window of a triangle formed by two A-site ions (e.g., K^+) and one B-site ion (e.g., Nb^{5+} and Mg^{2+}) to reach an adjacent oxygen vacant site.[31] It is reasonable that the static displacements of K^+ and neighboring Nb^{5+} or Mg^{2+} as well as the ordering distribution of Nb^{5+}/Mg^{2+} determine the window dimension and therefore strongly influence the activation energy and conductivity of oxide ion hopping in $KNb_{1-x}Mg_xO_{3-\delta}$. It is noted that the energy required for an oxide ion to pass through the window containing one Mg^{2+} will be larger than that in case of one Nb^{5+}. Increasing the symmetry of the perovskite structure allows a higher possibility for B-site Mg^{2+} or Nb^{5+} to be distributed at off-centers along ⟨111⟩.

(34) Li, G.; Mao, Y.; Li, L.; Feng, S.; Wang, M.; Yao, X. *Chem. Mater.* **1999**, *11*, 1259.
(35) Comes, R.; Lambert, M.; Guinier, A. *Solid State Commun.* **1968**, *6*, 715.
(36) Fitzgerald, J. J.; Huang, J.; Shore, J. S. *Ferroelectrics* **1999**, *233*, 187.
(37) Gourdain, D.; Moya, E.; Chervin, J. C.; Canny, B.; Pruzan, P. *Phys. Rev. B* **1995**, *52*, 3108.
(38) Dougherty, T. P.; Weiderrecht, G. P.; Nelson, K. A.; Garrett, M. H.; Jenssen, H. P.; Warde, C. *Phys. Rev. B* **1994**, *50*, 8996.
(39) (a) Laabidi, K.; Fontana, M. D.; Maglione, M.; Jannot, B.; Muller, K. A. *Europhys. Lett.* **1994**, *26*, 309. (b) Laabidi, K.; Fontana, M. D.; Jannot, B. *Solid State Commun.* **1990**, *76*, 765.
(40) Li, L.; Li, G.; Song, X.; Miao, J.; Zhou, X.; Su, W. *Chin. Phys. Lett.* **1998**, *15*, 925.
(41) Choi, S. M.; Lee, K. T.; Kim, S.; Chun, M. C.; Lee, H. L. *Solid State Ionics* **2000**, *131*, 221.

Correspondingly, the efficient dimension of the window for oxide ion hopping probably became narrowed. Therefore, an increase in activation energy could be expected for the cubic phase. Alternatively, the activation energy would be decreased if there was no obvious phase transitions to highly symmetric phases, as is found in $La_{0.9}Ba_{0.1}Ga_{1-x}Mg_xO_{3-y}$.[41] In the latter case, the total activation energy in the low-temperature range is the sum of the migration energy and the association energy. But the contribution of the activation energy term decreases at high temperatures. The increased conductivity for the cubic in Figure 9 can be explained by taking into account the destabilization of part of the defect associations or oxygen vacancy clusters at high temperatures. Some amount of mobile oxygen vacancies released gave rise to the passages for oxide ion hopping.

In regard to the relationship between conductivity and dopant content for $KNb_{1-x}Mg_xO_{3-\delta}$, the ordered distribution of B-site ions should be the main reason for the conductivity variations. According to the order−disorder transition model,[38] orthorhombic and tetragonal phases that appeared at temperatures below 400 °C had a relatively high order of Nb^{5+}/Mg^{2+} at B-sites. The ordered phases are usually less conductive and are transformed into the disordered phases of higher conductivity at higher temperatures.[42−44] The extremely large resistance associated with the ordered B-site ions in both orthorhombic and tetragonal phases makes it very difficult to measure full impedance semicircles over the entire frequency range of interest. Therefore, the relationship between phase transition and oxide ion conductivity could not be reached for orthorhombic to tetragonal to pseudocubic. The conductivity data for both pseudocubic and cubic phases in Table 1 can be rationalized as follows. For the pseudocubic phase, the content of oxygen vacancies increased with dopant content. At lower dopant content, most of these oxygen vacancies Vö were probably mobile. This could explain the gradual decrease of activation energy and increase of conductivity. At high dopant content, defect associations $\{Mg_{Nb}'''Vö\}$ localized near Mg^{2+} begin to form at the expense of the oxygen vacancies Vö. Correspondingly, oxygen sites near Nb^{5+} may become unavailable for hopping. This might explain the increase of activation energy and decrease of conductivity. The variations of the relative content of oxygen vacancies and defect associations could be used to explain the conductivity maximum at $x = 0.10$ and activation energy minimum at $x = \sim 0.05$. The dopant content for the conductivity maximum is closely related to the charge difference between the dopant ions and host ions. A large charge difference should give a conductivity maximum at a smaller dopant level because of the quick increase in the number of oxygen vacancies.[34] In this work, when the defect associations reached a maximum, the strong interactions among these defect associations in the pseudocubic lattice probably ordered the two oxygen vacancies localized near to the adjacent Mg^{2+} ions, while the rest of the oxygen vacancies became delocalized and therefore to some extent mobile, which probably accounts for the increase in conductivity and decrease in activation energy above $x = 0.25$.

For the cubic phase, the conductivity reached a maximum, while activation energy gave a minimum at a lower dopant content of $x = \sim 0.10$, which could be mainly due to the variation of relative content of oxygen vacancies Vö and defect associations $\{Mg_{Nb}'''Vö\}$ as those for the pseudocubic. When the dopant content was increased beyond $x = 0.15$, part of the defect associations $\{Mg_{Nb}'''Vö\}$ localized near Mg^{2+} became unstable under the strong interactions among the defect associations, leading to a transition of order−disorder for the defect associations $\{Mg_{Nb}'''Vö\}$, which accounted for the gradual increases in activation energy and ionic conductivity.

Conclusions

This paper reports on the preparation of oxide ion conductors $KNb_{1-x}Mg_xO_{3-\delta}$ ($x = 0.05-0.30$) by high temperature and pressure. There are clear advantages of the high-temperature and -pressure approach for single-step preparation of single-phase perovskites with Nb^{5+}/Mg^{2+} distributed at B-sites; e.g., the conditions suppress the formation of intermediate phases over those prepared by other synthetic routes. All $KNb_{1-x}Mg_xO_{3-\delta}$ ($x = 0.05-0.30$) samples were kinetically stable orthorhombic perovskite phase at ambient pressure. The lattice volume increased nonlinearly with the dopant content due to the substitution of Nb^{5+} by Mg^{2+}, variation of the relative content of oxygen vacancy and defect associations, and increase of lattice disorder of Nb^{5+}/Mg^{2+} at B-sites. At higher temperatures, $KNb_{1-x}Mg_xO_{3-\delta}$ exhibited phase transitions from orthorhombic to tetragonal, to pseudocubic, and then to cubic. Under the present experimental conditions, the conduction in the samples showed primarily ionic with extremely weak contributions from the p-type holes. $KNb_{0.90}Mg_{0.10}O_{2.85}$ was determined to be a highly conductive phase. The total conductivity data for $KNb_{1-x}Mg_xO_{3-\delta}$ gave two separated linear ranges with different variations of conductivity and activation energy, associating with the relative content of the oxygen vacancies and defect associations, and the order−disorder transitions.

Acknowledgment. This project is financially supported by a fund from NSFC (19804005) (L.L.). G.L. thanks Dr. S. M. Haile at Caltech for access to oxygen partial pressure impedance measurements.

CM020582E

(42) Tien, T. Y.; Subbarao, E. C. *J. Chem. Phys.* **1963**, *39*, 1041.
(43) Goodenough, J. B.; Ruiz-Diaz, J. E.; Zhen, Y. S. *Solid State Ionics* **1990**, *44*, 21.
(44) (a) Kendall, K. R.; Navas, C.; Thomas, J. K.; zur Loye, H. C. *Solid State Ionics* **1995**, *82*, 215. (b) Goodenough, J. B.; Manthiram, A.; Kuo, J. F. *Mater. Chem. Phys.* **1993**, *35*, 221.